

# Highly accurate electronic structure of metallic solids from coupled-cluster theory with nonperturbative triple excitations

Verena A. Neufeld<sup>1</sup> and Timothy C. Berkelbach<sup>1</sup>

<sup>1</sup>*Department of Chemistry, Columbia University, New York, New York 10027, USA*

(Dated: March 21, 2023)

Coupled-cluster theory with single, double, and perturbative triple excitations (CCSD(T))—often considered the “gold standard” of main-group quantum chemistry—is inapplicable to three-dimensional metals due to an infrared divergence, preventing its application to many important problems in materials science. We study the full, nonperturbative inclusion of triple excitations (CCSDT) and propose a new, iterative method, which we call ring-CCSDT, that resums the essential triple excitations with the same  $N^7$  run-time scaling as CCSD(T). CCSDT and ring-CCSDT are used to calculate the correlation energy of the uniform electron gas at metallic densities and the structural properties of solid lithium. Inclusion of connected triple excitations is shown to be essential to achieving high accuracy. We also investigate semiempirical CC methods based on spin-component scaling and the distinguishable cluster approximation and find that they enhance the accuracy of their parent *ab initio* methods.

*Introduction.* Accurately predicting energetic properties of metallic solids is crucial in computational materials science, with applications in heterogeneous catalysis, electrochemistry, and battery science [1–3]. Coupled-cluster theory with single and double excitations (CCSD) [4, 5] has recently been shown to provide reasonable energies for the uniform electron gas (UEG) [6–8] and for atomistic metallic solids, such as lithium and aluminum [9–12], but it does not reliably outperform density functional theory (DFT), which is significantly cheaper—some inclusion of connected triple excitations is clearly required. For non-metallic main-group solids, CCSD with perturbative triple excitations (CCSD(T)) [13] is highly accurate for bulk properties [14–18] and surface chemistry [18–22], mirroring its performance on molecules, where it commonly yields “chemical accuracy” of about 1 kcal/mol [5]. However, CCSD(T) is not expected to be applicable to three-dimensional metals: an approximate evaluation of the CCSD(T) energy of the UEG was shown to diverge in the thermodynamic limit [23], similar to the textbook result of second-order perturbation theory [24, 25].

Here, we investigate the accuracy of CC theory with non-perturbative triple excitations (CCSDT) to determine whether such a theory provides the desired accuracy for metals. Because the high cost of CCSDT limits its routine application, we also design and test lower cost alternatives. Below, we first review diagrammatic results on the ground-state energy of the UEG, including its high-density expansion, divergences and necessary resummations, and connections with coupled-cluster theory including double and triple excitations. An analysis of the (T) correction for the UEG motivates a new theory, which nonperturbatively retains the triple excitations necessary to preclude a divergence and which has the same  $N^7$  computational scaling as CCSD(T). We assess the performance of these methods with applications to the UEG at metallic densities and to solid lithium. Furthermore, we test several empirical modifications, including the distinguishable cluster (DC) approximation [26–28] and spin-component-scaled (SCS) CC theory [29–31], which were designed to approximate the effect of higher excitations without increasing

the computational cost.

*Diagrammatic results on the uniform electron gas.* The UEG, a model of interacting electrons in a uniform positive background, has been a famous testing ground for new developments in nonperturbative many-body quantum field theory. Specifically, the total energy of the UEG with electron density  $n$  has been evaluated to leading orders in the Wigner-Seitz radius  $r_s = (3/(4\pi n))^{1/3}$  [25, 32, 33], in the absence and presence of a spin polarization; in this work, we focus on the unpolarized case. The kinetic energy and Hartree-Fock exchange energy produce terms of  $O(r_s^{-2})$  and  $O(r_s^{-1})$ , respectively, and the remaining terms define the correlation energy.

From dimensionality arguments, it is expected that second-order perturbation theory contributes all terms of  $O(r_s^0)$ , which is correct for the second-order exchange energy [25, 34]. The second-order direct (ring) term, whose diagram is shown in Fig. 1(a), contributes a correlation energy  $E_{24} \propto r_s^0 \int_0^\infty dq f(q)/q^2$ , where

$$f(q) = \int_{|k+q|>1} d^3k \int_{|p+q|>1} d^3p \frac{\theta(1-k)\theta(1-p)}{q^2 + (\mathbf{k} + \mathbf{p}) \cdot \mathbf{q}} \quad (1)$$

and all dimensionless momenta  $\mathbf{k}, \mathbf{p}, \mathbf{q}$  are normalized to the Fermi momentum; we use the notation  $E_{m,2n}$  from Refs. 32 and 33, where  $m$  is the order in perturbation theory and  $n$  is the number of interactions with the same momentum transfer. It can be shown that  $f(q) \propto q$  in the limit  $q \rightarrow 0$ , and thus the second-order direct term famously diverges logarithmically. All higher order terms with the same ring structure ( $n$  rings at order  $n$  in perturbation theory), such as the one shown in Fig. 1(b) (i.e.,  $E_{36}$ ) exhibit the strongest divergences at each order, and their resummation to infinite order defines the random-phase approximation (RPA) [24, 25, 32, 33, 35–37],  $\varepsilon' = E_{24} + E_{36} + E_{48} + \dots$ . The RPA provides a correlation energy that is correct to  $O(\ln r_s)$  and is therefore exact in the high-density  $r_s \rightarrow 0$  limit (aside from a constant); the appearance of terms  $O(\ln r_s)$  in the density expansion signals the non-analyticity of the correlation energy. As is well-known, the CCSD energy contains all terms included in the RPA [38–40], providing a strong theoretical argument for the appli-

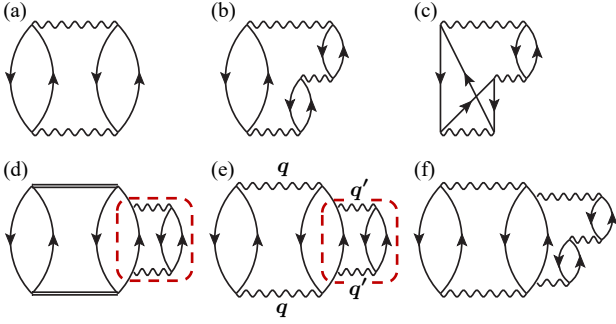


FIG. 1. Goldstone diagrams discussed in the text, which are included at various orders in perturbation theory and various flavors of CC theory. The dashed red box in (d) and (e) highlights the problematic feature responsible for the divergence of the CCSD(T) correlation energy.

cation of CC theories to metallic solids—a research agenda started more than 40 years ago [38, 39, 41, 42].

Third-order perturbation theory produces convergent terms that are  $O(r_s)$  (i.e.,  $E_{32}$ ), strongly divergent terms with three rings that are included in the RPA [i.e., Fig. 1(b) or  $E_{36}$ ], and more weakly divergent terms whose diagrams have only one ring, such as that shown in Fig. 1(c), which define  $E_{34}$ . These latter terms have to be resummed with higher-order divergent contributions that have analogous structure ( $n - 2$  rings at order  $n$  in perturbation theory),  $\varepsilon'' = E_{34} + E_{48} + \dots$ , which can be evaluated to identify a correlation energy that is exact to  $O(r_s, r_s \ln r_s)$  [32, 33, 43]. Remarkably, all of these terms are included in the CCSD correlation energy. Although it has long been appreciated that CCSD resums the most divergent terms that define the RPA correlation energy  $\varepsilon'$  [38–40], to the best of our knowledge, it has not been noted that it also resums these next most divergent terms that define  $\varepsilon''$ . Therefore,

$$f(\mathbf{q}, \mathbf{q}') = \int_{|\mathbf{k}+\mathbf{q}|>1} d^3k \int_{|\mathbf{m}+\mathbf{q}'>1} d^3m \int_{\substack{|\mathbf{p}+\mathbf{q}|>1 \\ |\mathbf{p}-\mathbf{q}'|<1}} d^3p \frac{\theta(1-k)\theta(1-p)\theta(1-m)}{[q^2 + (\mathbf{k} + \mathbf{p}) \cdot \mathbf{q}]^2 [q'^2 + (\mathbf{k} + \mathbf{p}) \cdot \mathbf{q} + (\mathbf{m} + \mathbf{p}) \cdot \mathbf{q}']}. \quad (2)$$

As usual, the correlation energy integral diverges due to the behavior of the integrand near  $\mathbf{q}, \mathbf{q}' = 0$ . Letting  $q_c$  be an infrared cutoff on both momentum integrals, the integrated result can be checked to diverge as  $O(q_c^{-2} \ln q_c)$ , demanding resummation with higher-order terms.

By replacing the outer Coulomb interactions by CCSD  $T_2$  amplitudes as in Fig. 1(d), CCSD(T) regularizes the integral over  $\mathbf{q}$ , but not  $\mathbf{q}'$ . This single ring diagram self-energy insertion, highlighted with a red box in Figs. 1(d) and (e), is responsible for the divergence of the CCSD(T) energy for metals. By analytically performing this regularization, the CCSD(T) energy can be shown to diverge as  $O(\ln q_c)$ , which is naturally weaker than that of bare fourth-order perturbation theory, but

CCSD is exact for the energy of the UEG to  $O(r_s, r_s \ln r_s)$ , which is one order higher than the RPA, in addition to recovering the correct constant term due to second-order exchange.

As expected, the CCSD energy is missing terms from fourth order in perturbation theory, including those that yield finite values of  $O(r_s^2)$  or that diverge weakly and must be resummed with higher-order terms. CCSDT produces an energy that is exact to fourth order in perturbation theory and includes resummations necessary to eliminate fourth-order divergences, thus providing a potentially powerful theory of the energy of metals. However, CCSDT has a high computational cost that scales as  $N^8$ , which precludes routine application to atomistic materials. Nonetheless, below we exploit the simplicity of the UEG and carefully designed composite corrections to provide the first estimates of the performance of CCSDT for the UEG in the thermodynamic limit and for solid lithium.

The intermediate theory CCSD(T), with a reduced  $N^7$  scaling, is very accurate for many molecules and insulating solids. However, CCSD(T) yields a divergent energy for metals, which was demonstrated numerically using an approximate form in Ref. 23. Here, we provide a diagrammatic analysis of the same behavior to shed more light on the failures of CCSD(T). Neglecting single excitations, which vanish for the UEG by symmetry, the energy correction in CCSD(T) is shown by the diagram in Fig. 1(d) (plus permutations due to exchange), where the double line indicates a converged CCSD  $T_2$  amplitude. To lowest order, the (T) correction is that of bare fourth-order perturbation theory, shown in Fig. 1(e), whose analysis elucidates the (T) divergence. Considering only the contribution without exchange, the problematic process has four interactions with two pairs of identical momenta exchanged,  $\mathbf{q}$  and  $\mathbf{q}'$ , i.e., the correlation energy is  $E_c \propto r_s^2 \int d^3q \int d^3q' f(\mathbf{q}, \mathbf{q}') / (q^4 q'^4)$ , where

still useless for quantitative calculations. This rate of divergence is exactly the same as that of second-order perturbation theory, which we exploit in the Supplemental Material [44] to numerically confirm the divergence of CCSD(T), along the lines of other works [45, 46].

Importantly, this analysis also identifies the minimal physics necessary to regularize the CCSD(T) approximation for metals, which is an infinite-order RPA-style resummation of ring diagrams in the self-energy insertion (like in the GW approximation [47]), as shown in Fig. 1(f). This can be achieved approximately by removing many of the terms from the CCSDT equations, analogous to the equivalence between (direct) ring-CCD and the RPA. This method, which we call

ring-CCSDT, is implemented as follows. The singles and doubles amplitude equations are exactly as in CCSDT. The triples amplitude equation is the same as in the CCSDT-1 approximation [4, 48–51], but is supplemented with direct ring diagrams,  $\epsilon_{ijk}^{abc} t_{ijk}^{abc} = R_{\text{CCSDT-1}} + R_{\text{dr}}$ ,

$$R_{\text{CCSDT-1}} = \hat{P}(k/ij|a/bc) \langle bc || dk \rangle t_{ij}^{ad} - \hat{P}(i/jk|c/ab) \langle lc || jk \rangle t_{il}^{ab} + \hat{P}(c/ab) (f_{cd} - \epsilon_c \delta_{cd}) t_{ijk}^{abd} - \hat{P}(k/ij) (f_{lk} - \epsilon_k \delta_{lk}) t_{ijl}^{abc} \quad (3a)$$

$$R_{\text{dr}} = \hat{P}(i/jk|a/bc) \langle al || id \rangle t_{ijk}^{abc} + \hat{P}(i/jk|abc) \langle lb || de \rangle t_{il}^{ad} t_{jk}^{ec} - \hat{P}(ijk|a/bc) \langle lm || dj \rangle t_{il}^{ad} t_{mk}^{bc} + \hat{P}(i/jk|a/bc) \langle lm || de \rangle t_{il}^{ad} t_{mjk}^{ebc} \quad (3b)$$

where  $\hat{P}(k/ij|a/bc) = [1 - \hat{P}(ik) - \hat{P}(jk)][1 - \hat{P}(ab) - \hat{P}(ac)]$  and  $\hat{P}(ij)$  generates the permutation of  $i$  and  $j$  (as usual,  $\epsilon_{ijk}^{abc}$  is an orbital energy denominator,  $f_{pq}$  is a Fock matrix element,  $i, j, k, l, m$  indicate occupied spin orbitals,  $a, b, c, d, e$  unoccupied spin orbitals, Coulomb integrals are in  $\langle 12 || 12 \rangle$  notation, the double bar indicates antisymmetrized integrals, and summation over repeated indices  $l, m, d, e$  is implied).

Unfortunately, despite its iterative nature, the CCSDT-1 approximation (without the ring diagrams) is a divergent theory of metals, like CCSD(T), because of the isolated ring diagram highlighted in Figs. 1(d) and (e). In the ring-CCSDT approximation, not all time-orderings of repeated ring diagrams are included: all forward (Tamm-Dancoff) time-orderings are included, which is sufficient to preclude a divergence [38], and a subset of the non-Tamm-Dancoff time-orderings are included, but not all those corresponding to the complete RPA; this is very similar to the diagrammatic content of the coupled-cluster Green’s function [52, 53]. To include all time-orderings that define RPA screening would require inclusion of connected quadruple excitations.

The first and last terms of  $R_{\text{dr}}$  exhibit  $N^8$  computational scaling, like the parent CCSDT method. However, the use of direct (non-antisymmetrized) ring diagrams enables a reduction in scaling with the use of density-fitting (or Cholesky decomposition) of the Coulomb integrals  $\langle pq || rs \rangle = \sum_P L_{pr}^P L_{qs}^P$ , where  $P$  is an auxiliary index. For example, the last term can be constructed as

$$\sum_{lmde} \langle lm || de \rangle t_{il}^{ad} t_{mjk}^{ebc} = \sum_P \left[ \sum_{ld} L_{ld}^P t_{il}^{ad} \right] \left[ \sum_{me} L_{me}^P t_{mjk}^{ebc} \right]. \quad (4)$$

With such a compression of the Coulomb integrals, ring-CCSDT is an iterative  $N^7$  method, providing an appealing alternative to the CCSD(T) approximation that is applicable to metals (although the storage of the  $T_3$  amplitudes is a separate bottleneck).

*Results for the UEG.* CC approximations are difficult to treat semi-analytically, even for the UEG. Therefore, we simulate a UEG of electron density  $n$  via a cubic box of  $N$  electrons with volume  $V = N/n = (4/3)\pi r_s^3 N$  and a plane-wave orbital basis. Although several improved CC methods have been previously applied to UEG models containing a finite

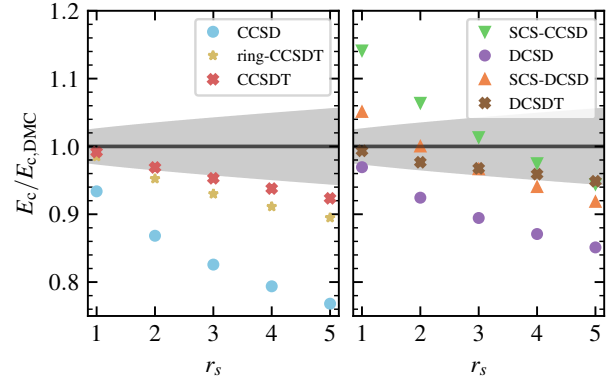


FIG. 2. Ratio of the coupled-cluster correlation energy to the diffusion Monte Carlo (DMC) correlation energy [54, 55] for the three-dimensional UEG with  $r_s = 1-5$ , as given by the methods indicated in the legend. The methods are separated into those that are purely diagrammatic (left) and those that are semi-empirical (right). Range of chemical accuracy ( $\pm 1$  kcal/mol or  $\pm 1.6$   $mE_h$ ) is shown with a grey shaded area.

number of electrons [56–59], here we are concerned with the critical question of their performance in the thermodynamic limit, which we estimate via basis set corrections and extrapolations to the thermodynamic limit. Specifically, we perform CCSD and DCSD calculations on systems containing up to  $N = 1404$  electrons and estimate the complete basis set limit using calculations on smaller system sizes. These results are then used to extrapolate to the thermodynamic limit assuming that finite-size errors in the correlation energy decay asymptotically as  $N^{-2/3}$ —a functional form that has also been proposed in recent work [60]. Our final CCSD correlation energies agree within about 1  $mE_h$  with previous studies that targeted the thermodynamic limit [6, 7], despite different technical details, providing a validation of our methods. CCSDT, ring-CCSDT, and DCSDT calculations are performed on systems containing up to  $N = 156$  electrons, and we calculate the energy difference with respect to DCSD. The complete basis set limit of this energy difference is estimated based on smaller values of  $N$  and then extrapolated to the thermodynamic limit. Additional technical details are given in the Supplemental Material [44].

In Fig. 2, we present the correlation energy of the UEG at metallic densities of  $r_s = 1-5$  from various CC theories as a fraction of the numerically exact result, estimated via the Perdew-Zunger fit [55] to diffusion Monte Carlo (DMC) results [54]; a table of all values is given in the Supplemental Material [44]. The magnitude of the DMC correlation energy ranges from 60  $mE_h$  at  $r_s = 1$  to 28  $mE_h$  at  $r_s = 5$ . As expected based on the density expansion discussed above, the relative accuracy of diagrammatic methods shown in Fig. 2(a) (CCSD, CCSDT, and ring-CCSDT) decreases with increasing  $r_s$ . Compared to CCSD, which recovers only about 75–95% of the DMC correlation energy, CCSDT performs extremely well and recovers between 99% (at  $r_s = 1$ ) and 92%

(at  $r_s = 5$ ), corresponding to an absolute accuracy of 0.5–2.2  $mE_h$ . The good performance of ring-CCSDT, with errors of 0.9–3.0  $mE_h$ , shows that the same ring diagram resummation responsible for curing the divergence of CCSD(T) is also responsible for most of the correlation energy associated with connected triple excitations.

The semi-empirical CC methods shown in Fig. 2(b) (SCS-CCSD, DCSD, SCS-DCSD, and DCSDT) typically perform better than their parent diagrammatic method. SCS-CCSD [30] improves over CCSD, except at small  $r_s$ , demonstrating that semi-empirical modifications can spoil valuable formal properties like the exactness of CC theories in the high-density limit. DCSD [26] is better behaved and roughly halves the error of CCSD over this density range. SCS-DCSD [31] is a further improvement and provides the best overall performance of the  $N^6$  scaling methods. Remarkably, DCSDT [27, 28] yields results of extremely high accuracy, recovering more than 94% of the DMC correlation energy at all densities, which corresponds to an error of less than 1.6  $mE_h$ , i.e., under 1 kcal/mol.

*Results on solid lithium.* Next, we investigate the transferability of the above performance to a real material. We study solid lithium, which is a simple metal with a valence electron density corresponding to  $r_s \approx 3.2$ . We use CCSD, DCSD, ring-CCSDT, CCSDT, and DCSDT to calculate the equilibrium lattice parameter, bulk modulus, and cohesive energy. All calculations were performed with a development branch of PySCF [61–63], and all technical details—such as pseudopotentials, basis sets (up to quadruple-zeta Gaussian type orbitals), and Brillouin zone samplings (up to 64  $k$ -points, plus extrapolation)—are the same as in our previous work [11]; in that work, we found that CCSD predictions had significant room for improvement (at the CCSD level, we find that our updated finite-size extrapolations cause only small differences from our previous work, e.g., about 0.8  $mE_h$  in the cohesive energy). We estimate the ring-CCSDT, CCSDT, and DCSDT energies using composite corrections, by again considering the differences to DCSD, based on calculations with small supercells (containing 8 and 16 Li atoms), frozen core orbitals, and frozen virtual natural orbitals [44].

Results are presented in Fig. 3, where they are compared to low temperature experimental results [64–67] that have been corrected for zero-point vibrational effects based on HSE06 phonon calculations [64]; a table of all values is given in the Supplemental Material [44]. Consistent with our results on the UEG, we see relatively systematic improvement with increasing sophistication of the theory. DCSD, ring-CCSDT, CCSDT, and DCSDT are all improvements over CCSD and they achieve accuracies of 0.004–0.02 Å, 0.1–0.2 GPa, and 4–6  $mE_h$  in the lattice constant, bulk modulus, and cohesive energy, respectively. It is hard to disentangle the remaining discrepancies, which likely include some combination of pseudopotential, basis set, and finite-size error, incomplete correlation, and experimental uncertainty, including vibrational corrections. We also compare to DFT results reported in Ref. [64] using the LDA [68] and HSE06 [69–71]

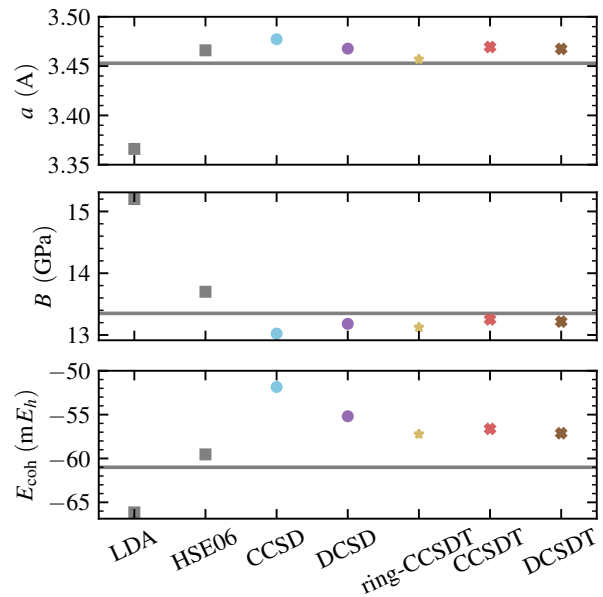


FIG. 3. Equilibrium lattice constant  $a$ , bulk modulus  $B$ , and cohesive energy  $E_{\text{coh}}$  for solid lithium. Results are shown at the indicated levels of CC theory and compared to experimental results [64–67] (solid horizontal lines), which have been corrected for zero-point vibrational energy using the HSE06 corrections from Ref. 64. DFT results for the LDA and HSE06 functionals are shown for comparison (from Ref. 64)

functionals. While the LDA functional does not predict accurate structural properties (despite its exactness for the UEG), the HSE06 functional performs very well. Importantly, we see that the improved methods explored in this work clearly outperform CCSD, bringing CC theory in line with the best performing DFT functionals.

*Conclusion.* Despite the apparent simplicity of simple metals, including the uniform electron gas, achieving high accuracy for the electron correlation energy with *ab initio* wavefunction or diagrammatic methods is clearly a challenge. We have shown that within the family of CC theories, the infinite-order inclusion of connected triple excitations is essential, although semi-empirical treatments of these effects are surprisingly effective. We expect that the methods explored here, which have been evaluated for their ability to predict the properties of nearly uniform systems, will outperform DFT for more heterogeneous systems, such as those arising in surface chemistry. Before CC methods are widely used in this context, their comparatively high computational and storage costs must be addressed. However, in the meantime, they can be used to provide predictions of benchmark quality, especially in the many situations where experimental values cannot be obtained to the required precision.

*Acknowledgments.* We thank James Callahan and Xiao Wang for helpful discussions. This work was supported by the

Columbia Center for Computational Electrochemistry and the National Science Foundation under Grant No. CHE-1848369. We acknowledge computing resources from Columbia University's Shared Research Computing Facility project, which is supported by NIH Research Facility Improvement Grant 1G20RR030893-01, and associated funds from the New York State Empire State Development, Division of Science Technology and Innovation (NYSTAR) Contract C090171, both awarded April 15, 2010. Data analysis and visualization were performed using NumPy [72], SciPy [73], pandas [74], Matplotlib [75], seaborn [76], and JaxoDraw [77]. UEG calculations used Julia [78], Fermi.jl [79], TensorOperations.jl [80], and Tullio.jl [81].

- 
- [1] J. K. Nørskov, F. Abild-Pedersen, F. Studt, and T. Bligaard, Density functional theory in surface chemistry and catalysis, *Proc. Natl. Acad. Sci.* **108**, 937 (2011).
- [2] F. Calle-Vallejo and M. T. M. Koper, First-principles computational electrochemistry: Achievements and challenges, *Electrochim. Acta* **84**, 3 (2012).
- [3] Q. He, B. Yu, Z. Li, and Y. Zhao, Density Functional Theory for Battery Materials, *Energy Environ. Sci.* **2**, 264 (2019).
- [4] I. Shavitt and R. J. Bartlett, *Many-Body Methods in Chemistry and Physics: MBPT and Coupled-Cluster Theory*, Cambridge Molecular Science (Cambridge University Press, Cambridge, 2009).
- [5] R. J. Bartlett and M. Musiał, Coupled-cluster theory in quantum chemistry, *Rev. Mod. Phys.* **79**, 291 (2007).
- [6] J. J. Shepherd, Communication: Convergence of many-body wave-function expansions using a plane-wave basis in the thermodynamic limit, *J. Chem. Phys.* **145**, 031104 (2016).
- [7] T. N. Mihm, B. Yang, and J. J. Shepherd, Power Laws Used to Extrapolate the Coupled Cluster Correlation Energy to the Thermodynamic Limit, *J. Chem. Theor. Comput.* **17**, 2752 (2021).
- [8] J. M. Callahan, M. F. Lange, and T. C. Berkelbach, Dynamical correlation energy of metals in large basis sets from downfolding and composite approaches, *J. Chem. Phys.* **154**, 211105 (2021).
- [9] H. Stoll, B. Paulus, and P. Fulde, An incremental coupled-cluster approach to metallic lithium, *Chem. Phys. Lett.* **469**, 90 (2009).
- [10] T. N. Mihm, T. Schäfer, S. K. Ramadugu, L. Weiler, A. Grüneis, and J. J. Shepherd, A shortcut to the thermodynamic limit for quantum many-body calculations of metals, *Nat. Comput. Sci.* **1**, 801 (2021).
- [11] V. A. Neufeld, H.-Z. Ye, and T. C. Berkelbach, Ground-State Properties of Metallic Solids from Ab Initio Coupled-Cluster Theory, *J. Phys. Chem. Lett.* **13**, 7497 (2022).
- [12] L. Weiler, T. N. Mihm, and J. J. Shepherd, Machine learning for a finite size correction in periodic coupled cluster theory calculations, *J. Chem. Phys.* **156**, 204109 (2022).
- [13] K. Raghavachari, G. W. Trucks, J. A. Pople, and M. Head-Gordon, A fifth-order perturbation comparison of electron correlation theories, *Chem. Phys. Lett.* **157**, 479 (1989).
- [14] P. Schwerdtfeger, B. Assadollahzadeh, and A. Hermann, Convergence of the Møller-Plesset perturbation series for the fcc lattices of neon and argon, *Phys. Rev. B* **82**, 205111 (2010).
- [15] G. H. Booth, A. Grüneis, G. Kresse, and A. Alavi, Towards an exact description of electronic wavefunctions in real solids, *Nature* **493**, 365 (2013).
- [16] A. Grüneis, A coupled cluster and Møller-Plesset perturbation theory study of the pressure induced phase transition in the LiH crystal, *J. Chem. Phys.* **143**, 102817 (2015).
- [17] T. Gruber, K. Liao, T. Tsatsoulis, F. Hummel, and A. Grüneis, Applying the Coupled-Cluster Ansatz to Solids and Surfaces in the Thermodynamic Limit, *Phys. Rev. X* **8**, 021043 (2018).
- [18] T. Gruber and A. Grüneis, *Ab initio* calculations of carbon and boron nitride allotropes and their structural phase transitions using periodic coupled cluster theory, *Phys. Rev. B* **98**, 134108 (2018).
- [19] T. Tsatsoulis, F. Hummel, D. Usvyat, M. Schütz, G. H. Booth, S. S. Binnie, M. J. Gillan, D. Alfè, A. Michaelides, and A. Grüneis, A comparison between quantum chemistry and quantum Monte Carlo techniques for the adsorption of water on the (001) LiH surface, *J. Chem. Phys.* **146**, 204108 (2017).
- [20] T. Tsatsoulis, S. Sakong, A. Groß, and A. Grüneis, Reaction energetics of hydrogen on Si(100) surface: A periodic many-electron theory study, *J. Chem. Phys.* **149**, 244105 (2018).
- [21] J. G. Brandenburg, A. Zen, M. Fitzner, B. Ramberger, G. Kresse, T. Tsatsoulis, A. Grüneis, A. Michaelides, and D. Alfè, Physisorption of Water on Graphene: Subchemical Accuracy from Many-Body Electronic Structure Methods, *J. Phys. Chem. Lett.* **10**, 358 (2019).
- [22] B. T. G. Lau, G. Knizia, and T. C. Berkelbach, Regional Embedding Enables High-Level Quantum Chemistry for Surface Science, *J. Phys. Chem. Lett.* **12**, 1104 (2021).
- [23] J. J. Shepherd and A. Grüneis, Many-Body Quantum Chemistry for the Electron Gas: Convergent Perturbative Theories, *Phys. Rev. Lett.* **110**, 226401 (2013).
- [24] W. Macke, Über die Wechselwirkungen im Fermi-Gas. Polarisationserscheinungen, Correlationsenergie, Elektronenkondensation, *Z. Naturforsch. A* **5**, 192 (1950), publisher: De Gruyter.
- [25] M. Gell-Mann and K. A. Brueckner, Correlation Energy of an Electron Gas at High Density, *Phys. Rev.* **106**, 364 (1957).
- [26] D. Kats and F. R. Manby, Communication: The distinguishable cluster approximation, *J. Chem. Phys.* **139**, 021102 (2013).
- [27] D. Kats and A. Köhn, On the distinguishable cluster approximation for triple excitations, *J. Chem. Phys.* **150**, 151101 (2019).
- [28] V. Rishi and E. F. Valeev, Can the distinguishable cluster approximation be improved systematically by including connected triples?, *J. Chem. Phys.* **151**, 064102 (2019).
- [29] S. Grimme, Improved second-order Møller-Plesset perturbation theory by separate scaling of parallel- and antiparallel-spin pair correlation energies, *J. Chem. Phys.* **118**, 9095 (2003).
- [30] T. Takatani, E. G. Hohenstein, and C. D. Sherrill, Improvement of the coupled-cluster singles and doubles method via scaling same- and opposite-spin components of the double excitation correlation energy, *J. Chem. Phys.* **128**, 124111 (2008).
- [31] D. Kats, Improving the distinguishable cluster results: spin-component scaling, *Mol. Phys.* **116**, 1435 (2018).
- [32] W. J. Carr and A. A. Maradudin, Ground-State Energy of a High-Density Electron Gas, *Phys. Rev.* **133**, A371 (1964).
- [33] T. Endo, M. Horiuchi, Y. Takada, and H. Yasuhara, High-density expansion of correlation energy and its extrapolation to the metallic density region, *Phys. Rev. B* **59**, 7367 (1999).
- [34] L. Onsager, L. Mittag, and M. J. Stephen, Integrals in the Theory of Electron Correlations, *Ann. Phys.* **473**, 71 (1966).
- [35] D. Bohm and D. Pines, A Collective Description of Electron Interactions. I. Magnetic Interactions, *Phys. Rev.* **82**, 625 (1951).
- [36] D. Pines and D. Bohm, A Collective Description of Electron Interactions: II. Collective vs Individual Particle Aspects of the Interactions, *Phys. Rev.* **85**, 338 (1952).

- [37] D. Bohm and D. Pines, A Collective Description of Electron Interactions: III. Coulomb Interactions in a Degenerate Electron Gas, *Phys. Rev.* **92**, 609 (1953).
- [38] D. L. Freeman, Coupled-cluster expansion applied to the electron gas: Inclusion of ring and exchange effects, *Phys. Rev. B* **15**, 5512 (1977).
- [39] R. F. Bishop and K. H. Lührmann, Electron correlations: I. Ground-state results in the high-density regime, *Phys. Rev. B* **17**, 3757 (1978).
- [40] G. E. Scuseria, T. M. Henderson, and D. C. Sorensen, The ground state correlation energy of the random phase approximation from a ring coupled cluster doubles approach, *J. Chem. Phys.* **129**, 231101 (2008).
- [41] R. F. Bishop and K. H. Lührmann, Electron correlations. II. Ground-state results at low and metallic densities, *Phys. Rev. B* **26**, 5523 (1982).
- [42] K. Emrich and J. G. Zabolitzky, Electron correlations in the Bogoljubov coupled-cluster formalism, *Phys. Rev. B* **30**, 2049 (1984).
- [43] D. F. DuBois, Electron interactions: Part II. Properties of a dense electron gas, *Ann. Phys.* **8**, 24 (1959).
- [44] See Supplemental Material at [URL will be inserted by publisher] for technical details of all calculations and a discussion of finite-size errors in metals, including numerical demonstration of convergent and divergent behaviors of the considered theories.
- [45] J. J. Shepherd, T. M. Henderson, and G. E. Scuseria, Range-Separated Brueckner Coupled Cluster Doubles Theory, *Phys. Rev. Lett.* **112**, 133002 (2014).
- [46] J. J. Shepherd, T. M. Henderson, and G. E. Scuseria, Coupled cluster channels in the homogeneous electron gas, *J. Chem. Phys.* **140**, 124102 (2014).
- [47] L. Hedin, New Method for Calculating the One-Particle Green's Function with Application to the Electron-Gas Problem, *Phys. Rev.* **139**, A796 (1965).
- [48] Y. S. Lee and R. J. Bartlett, A study of  $\text{Be}_2$  with many-body perturbation theory and a coupled-cluster method including triple excitations, *J. Chem. Phys.* **80**, 4371 (1984).
- [49] Y. S. Lee, S. A. Kucharski, and R. J. Bartlett, A coupled cluster approach with triple excitations, *J. Chem. Phys.* **81**, 5906 (1984).
- [50] M. Urban, J. Noga, S. J. Cole, and R. J. Bartlett, Towards a full CCSDT model for electron correlation, *J. Chem. Phys.* **83**, 4041 (1985).
- [51] J. Noga, R. J. Bartlett, and M. Urban, Towards a full CCSDT model for electron correlation. CCSDT-n models, *Chem. Phys. Lett.* **134**, 126 (1987).
- [52] M. F. Lange and T. C. Berkelbach, On the Relation between Equation-of-Motion Coupled-Cluster Theory and the *GW* Approximation, *J. Chem. Theor. Comput.* **14**, 4224 (2018).
- [53] J. Tölle and G. K.-L. Chan, Exact relationships between the *GW* approximation and equation-of-motion coupled-cluster theories through the quasi-boson formalism, [arXiv:2212.08982 \[cond-mat, physics:physics\]](https://arxiv.org/abs/2212.08982) (2022).
- [54] D. M. Ceperley and B. J. Alder, Ground State of the Electron Gas by a Stochastic Method, *Phys. Rev. Lett.* **45**, 566 (1980).
- [55] J. P. Perdew and A. Zunger, Self-interaction correction to density-functional approximations for many-electron systems, *Phys. Rev. B* **23**, 5048 (1981).
- [56] J. McClain, J. Lischner, T. Watson, D. A. Matthews, E. Ronca, S. G. Louie, T. C. Berkelbach, and G. K.-L. Chan, Spectral functions of the uniform electron gas via coupled-cluster theory and comparison to the *G W* and related approximations, *Phys. Rev. B* **93**, 235139 (2016).
- [57] J. S. Spencer and A. J. W. Thom, Developments in stochastic coupled cluster theory: The initiator approximation and application to the uniform electron gas, *J. Chem. Phys.* **144**, 084108 (2016).
- [58] V. A. Neufeld and A. J. W. Thom, A study of the dense uniform electron gas with high orders of coupled cluster, *J. Chem. Phys.* **147**, 194105 (2017).
- [59] K. Liao, T. Schraivogel, H. Luo, D. Kats, and A. Alavi, Towards efficient and accurate *ab initio* solutions to periodic systems via transcorrelation and coupled cluster theory, *Phys. Rev. Res.* **3**, 033072 (2021).
- [60] T. N. Mihm, L. Weiler, and J. J. Shepherd, How the Exchange Energy Can Affect the Power Laws Used to Extrapolate the Coupled Cluster Correlation Energy to the Thermodynamic Limit, *J. Chem. Theor. Comput.* [10.1021/acs.jctc.2c00737](https://doi.org/10.1021/acs.jctc.2c00737) (2023).
- [61] Q. Sun, Libcint: An efficient general integral library for Gaussian basis functions, *J. Comput. Chem.* **36**, 1664 (2015).
- [62] Q. Sun, T. C. Berkelbach, N. S. Blunt, G. H. Booth, S. Guo, Z. Li, J. Liu, J. D. McClain, E. R. Sayfutyarova, S. Sharma, S. Wouters, and G. K.-L. Chan, PySCF: the Python-based simulations of chemistry framework, *WIREs Comput. Mol. Sci.* **8**, e1340 (2018).
- [63] Q. Sun, X. Zhang, S. Banerjee, P. Bao, M. Barbry, N. S. Blunt, N. A. Bogdanov, G. H. Booth, J. Chen, Z.-H. Cui, J. J. Eriksen, Y. Gao, S. Guo, J. Hermann, M. R. Hermes, K. Koh, P. Koval, S. Lehtola, Z. Li, J. Liu, N. Mardirossian, J. D. McClain, M. Motta, B. Mussard, H. Q. Pham, A. Pulkin, W. Purwanto, P. J. Robinson, E. Ronca, E. R. Sayfutyarova, M. Scheurer, H. F. Schurkus, J. E. T. Smith, C. Sun, S.-N. Sun, S. Upadhyay, L. K. Wagner, X. Wang, A. White, J. D. Whitfield, M. J. Williamson, S. Wouters, J. Yang, J. M. Yu, T. Zhu, T. C. Berkelbach, S. Sharma, A. Y. Sokolov, and G. K.-L. Chan, Recent developments in the PySCF program package, *J. Chem. Phys.* **153**, 024109 (2020).
- [64] G.-X. Zhang, A. M. Reilly, A. Tkatchenko, and M. Scheffler, Performance of various density-functional approximations for cohesive properties of 64 bulk solids, *New J. Phys.* **20**, 063020 (2018).
- [65] R. Berliner and S. A. Werner, Effect of stacking faults on diffraction: The structure of lithium metal, *Phys. Rev. B* **34**, 3586 (1986).
- [66] R. A. Felice, J. Trivisonno, and D. E. Schuele, Temperature and pressure dependence of the single-crystal elastic constants of Li 6 and natural lithium, *Phys. Rev. B* **16**, 5173 (1977).
- [67] C. Kittel, *Introduction to solid state physics*, 8th ed. (John Wiley & Sons, Inc., 2005).
- [68] W. Kohn and L. J. Sham, Self-consistent equations including exchange and correlation effects, *Phys. Rev.* **140**, A1133 (1965).
- [69] J. Heyd, G. E. Scuseria, and M. Ernzerhof, Hybrid functionals based on a screened Coulomb potential, *J. Chem. Phys.* **118**, 8207 (2003).
- [70] J. Heyd, G. E. Scuseria, and M. Ernzerhof, Erratum: "Hybrid functionals based on a screened Coulomb potential" [*J. Chem. Phys.* **118**, 8207 (2003)], *J. Chem. Phys.* **124**, 219906 (2006).
- [71] A. V. Krkavau, O. A. Vydrov, A. F. Izmaylov, and G. E. Scuseria, Influence of the exchange screening parameter on the performance of screened hybrid functionals, *J. Chem. Phys.* **125**, 224106 (2006).
- [72] C. R. Harris, K. J. Millman, S. J. van der Walt, R. Gommers, P. Virtanen, D. Cournapeau, E. Wieser, J. Taylor, S. Berg, N. J. Smith, R. Kern, M. Picus, S. Hoyer, M. H. van Kerkwijk, M. Brett, A. Haldane, J. F. del Río, M. Wiebe, P. Peterson,

- P. Gérard-Marchant, K. Sheppard, T. Reddy, W. Weckesser, H. Abbasi, C. Gohlke, and T. E. Oliphant, Array programming with NumPy, *Nature* **585**, 357 (2020).
- [73] SciPy 1.0 Contributors, P. Virtanen, R. Gommers, T. E. Oliphant, M. Haberland, T. Reddy, D. Cournapeau, E. Burovski, P. Peterson, W. Weckesser, J. Bright, S. J. van der Walt, M. Brett, J. Wilson, K. J. Millman, N. Mayorov, A. R. J. Nelson, E. Jones, R. Kern, E. Larson, C. J. Carey, I. Polat, Y. Feng, E. W. Moore, J. VanderPlas, D. Laxalde, J. Perktold, R. Cimrman, I. Henriksen, E. A. Quintero, C. R. Harris, A. M. Archibald, A. H. Ribeiro, F. Pedregosa, and P. van Mulbregt, SciPy 1.0: fundamental algorithms for scientific computing in Python, *Nature Methods* **17**, 261 (2020).
- [74] W. McKinney, Data structures for statistical computing in python, in *Proceedings of the 8th Python in Science Conference*, edited by S. van der Walt and J. Millman (2009) pp. 55 – 61.
- [75] J. D. Hunter, Matplotlib: A 2d graphics environment, *Comput. Sci. Eng.* **9**, 90 (2007).
- [76] M. L. Waskom, seaborn: statistical data visualization, *J. Open Source Softw.* **6**, 3021 (2021).
- [77] D. Binosi and L. Theußl, JaxoDraw: A graphical user interface for drawing Feynman diagrams, *Comput. Phys. Commun.* **161**, 76 (2004).
- [78] J. Bezanson, A. Edelman, S. Karpinski, and V. B. Shah, Julia: A Fresh Approach to Numerical Computing, *SIAM Rev.* **59**, 65 (2017).
- [79] G. J. R. Aroeira, M. M. Davis, J. M. Turney, and H. F. Schaefer III, Fermi.jl: A Modern Design for Quantum Chemistry, *J. Chem. Theor. Comput.* **18**, 677 (2022).
- [80] TensorOperations.jl (), <https://github.com/Jutho/TensorOperations.jl>, accessed 2023-02-13.
- [81] Tullio.jl (), <https://github.com/mcabbott/Tullio.jl>, accessed 2023-02-13.

# Supplemental Material for: Highly accurate electronic structure of metallic solids from coupled-cluster theory with nonperturbative triple excitations

Verena A. Neufeld<sup>1</sup> and Timothy C. Berkelbach<sup>1</sup>

<sup>1</sup>*Department of Chemistry, Columbia University, New York, New York 10027, USA*

(Dated: March 21, 2023)

## S1. UNIFORM ELECTRON GAS CALCULATIONS

In a plane-wave basis, the Hamiltonian of the uniform electron gas (UEG) in a cubic box of volume  $V = L^3$  is

$$H = \sum_{\mathbf{k}\sigma} \epsilon_{\mathbf{k}} a_{\mathbf{k},\sigma}^{\dagger} a_{\mathbf{k},\sigma} + \frac{1}{2} \sum_{\mathbf{k}_1\sigma_1, \mathbf{k}_2\sigma_2} \sum_{\mathbf{q}\neq 0} v(\mathbf{q}) a_{\mathbf{k}_1+\mathbf{q},\sigma_1}^{\dagger} a_{\mathbf{k}_2-\mathbf{q},\sigma_2}^{\dagger} a_{\mathbf{k}_2,\sigma_2} a_{\mathbf{k}_1,\sigma_1} \quad (\text{S1})$$

$$v(\mathbf{q}) = \begin{cases} 4\pi e^2 / (Vq^2) & q \neq 0 \\ v_{\text{M}} & q = 0 \end{cases} \quad (\text{S2})$$

where  $v_{\text{M}} \propto L^{-1}$  is the Madelung constant of the cell,  $\epsilon_{\mathbf{k}} = \hbar^2 k^2 / (2m)$ ,  $\mathbf{k} = (2\pi/L)[n_x, n_y, n_z] + \mathbf{k}_s$  ( $n_i$  are integers), and  $\mathbf{k}_s$  is a shift of the  $k$ -point mesh consistent with twisted boundary conditions. Here we choose  $\mathbf{k}_s$  to be the Baldereschi point [1] of the cubic Brillouin zone, i.e.,  $\mathbf{k}_s = (2\pi/L)[1/4, 1/4, 1/4]$ , which we find to smooth the convergence to the thermodynamic limit (TDL). We study only closed-shell systems with “magic numbers” of electrons  $N$  increasing by roughly a factor of 2, i.e.,  $N = 14, 34, 70, \dots, 1404$ . CCSD-based and CCSDT-based calculations are performed using up to 1404 and 156 electrons, respectively. The box volume is based on the target density  $n$ , i.e.,  $V = N/n$ .

We note that the orbitals to be used in constructing *any* reference determinant without translational symmetry breaking, such as spin- or charge-density wave ordering, are just the plane-wave orbitals with the lowest kinetic energy. In “full” CC theories, such as CCSD or CCSDT, the final results depend only on this determinant of single-particle orbitals and *not* on their orbital energies. This point is important because the HF orbital energies are known to be problematic for metals. However, removing some terms from CC theory, as done in the (direct) RPA and ring-CCSDT, reintroduces a dependence on the orbital energies. The traditional RPA theory uses the kinetic energies only; for consistency with standard CC implementations, we use HF orbital energies in our ring-CCSDT calculations.

As a single-particle basis, we use  $M$  plane-wave spin-orbitals, where the largest value of  $M$  depends on  $N$ . Ultimately, we seek the combined complete basis set (CBS) limit and thermodynamic limit (TDL), which we describe in Sec. S1 B and S1 C. But first, we demonstrate the convergence and divergence behaviors with  $N$  of the CC theories discussed in the main text.

### A. Demonstration of convergence or divergence behaviors

In Fig. S1, we follow Refs. 2–4 and plot the correlation energy of CCSD(T), CCSDT-1, ring-CCSDT, and CCSDT against that of MP2 theory, with  $M/N \approx 1.5$  (i.e., the results are not in the CBS, but are sufficient to demonstrate the convergence or divergence with  $N$ ). More specifically, we plot the difference with respect to the CCSD correlation energy, which is known to converge with  $N$ . For CCSD(T), this difference is exactly the (T) correction, which we find to increase in linear proportion to the MP2 correlation energy, which is fully consistent with our analytical conclusion that both diverge logarithmically. We see that CCSDT-1 appears to diverge at least as fast as CCSD(T) and shows no indication of convergence at the accessible values of  $N$ . In contrast, ring-CCSDT and CCSDT show the onset of a plateau, providing strong numerical support for their convergence in the TDL, which is consistent with our expectations.

### B. Complete basis set limit estimation

For each  $N$ , we estimate the  $M \rightarrow \infty$  complete basis set (CBS) limit incrementally, using a composite correction based on the smaller value of  $N$  at the same level of theory,

$$E_N(\text{CBS}) \approx E_N(M) + E_{N/2}(\text{CBS}) - E_{N/2}(M/2), \quad (\text{S3})$$

where  $M$  is the largest value accessed for that value of  $N$ , “ $N/2$ ” is short-hand for the number of electrons that is *roughly* a factor of 2 smaller than  $N$ , and  $E_{N/2}(M/2)$  is found via interpolation of results with varying  $M$ , since we are limited to “magic



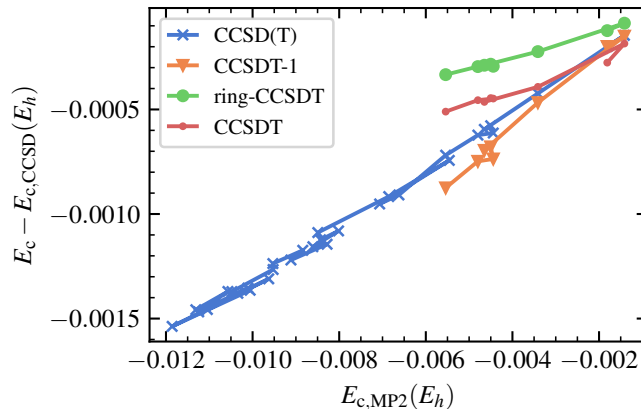


FIG. S1. Thermodynamic limit convergence at  $r_s = 4$  of the difference of the CCSD(T), CCSDT, CCSDT-1, and ring-CCSDT correlation energies to the CCSD correlation energy, plotted against the MP2 correlation energy. The ratio of the number of orbitals to number of electrons is  $M/N \approx 1.5$ , which is far from the complete basis set limit. Results are shown for systems ranging from ( $N = 34, M = 52$ ) to ( $N = 180, M = 272$ ) for CCSDT-1, ring-CCSDT, CCSDT, and up to ( $N = 628, M = 960$ ) for CCSD(T).

numbers” of basis functions. Table S1 shows, for each CC method, the maximum number of spin-orbitals  $M$  that we use for each number of electrons  $N$ .

For CCSD-based methods, we use Eq. (S3) to estimate the correlation energy  $E_c$ . For the more expensive CCSDT-based methods, we use Eq. (S3) to estimate the *difference* to the DCSD correlation energy,  $\Delta E_c(\text{XSDT} - \text{DCSD}) \equiv E_c(\text{XSDT}) - E_c(\text{DCSD})$ . In Fig. S2(a), we show the convergence of the incremental basis set corrections at  $r_s = 4$ , which can be seen to decrease in magnitude with increasing  $N$ . The final CBS energies and energy differences are then used to estimate the TDL, as described next.

### C. Thermodynamic limit extrapolation

Given CBS estimates at each value of  $N$ , we estimate the TDL by extrapolation. As justified in Sec. S2, we extrapolate the CCSD-based correlation energies by fitting to the functional form

$$E_c(N) = E_c(N \rightarrow \infty) + aN^{-2/3} + bN^{-1}, \quad (\text{S4})$$

where  $E_c(N)$  is the correlation energy per particle. In practice, we fit to the six data points with the largest  $N$ . For CCSDT-based methods, we extrapolate the CBS estimate of the *difference* to DCSD, as described in the previous section. Because the  $N^{-2/3}$  term in Eq. (S4) is attributed to the HF exchange energy, which should cancel in the difference of two correlated energies, we extrapolate these differences using only  $N^{-1}$ , i.e., with  $a = 0$ ; specifically, a two-point extrapolation is performed with  $N = 34$  and  $N = 70$ . We then add this difference to the combined CBS+TDL value of the DCSD correlation energy to obtain our final estimate of the CBS+TDL value of the CCSDT-based correlation energies. Figure S2(b) shows the TDL convergence at  $r_s = 4$  for the correlation energy of CCSD and DCSD and for the correlation energy difference of various CCSDT-based methods.

	$N = 14$	$N = 34$	$N = 70$	$N = 156$	$N = 332$	$N = 700$	$N = 1404$
CCSD	47118	23966	10332	5252	2488	2392	2392
DCSD	52746	27154	19962	8646	4850	3996	4140
CCSDT	1476–1538	832	502	344	-	-	-
ring-CCSDT	5720	1676	1104	302–410	-	-	-
DCSDT	1476	796–832	464–502	272–344	-	-	-

TABLE S1. Maximum number of spin-orbitals  $M$  for given number of electrons  $N$  for the CC methods. The maximum number of spin-orbitals  $M$  sometimes depends on  $r_s$ , in which case a range is given.

## D. Final Results

Combining the extrapolations described above yields our final correlation energy estimates in the CBS and TDL limits, which are given in Tab. S2 and were presented graphically in Fig. 1 of the main text.

	$E_c/N$ ( $mE_h$ )				
	$r_s = 1$	$r_s = 2$	$r_s = 3$	$r_s = 4$	$r_s = 5$
CCSD	-56	-39	-31	-25	-22
CCSDT	-59	-44	-35	-30	-26
ring-CCSDT	-59	-43	-35	-29	-25
SCS-CCSD	-68	-48	-38	-31	-27
DCSD	-58	-42	-33	-28	-24
SCS-DCSD	-63	-45	-36	-30	-26
DCSDT	-59	-44	-36	-31	-27
DMC [5, 6]	-60	-45	-37	-32	-28

TABLE S2. Uniform electron gas correlation energy per electron for  $r_s = 1 - 5$  from various coupled cluster methods extrapolated to the complete basis set and thermodynamic limit. (Fitted) diffusion Monte Carlo (DMC) results [5, 6] are shown for comparison.

### S2. MANY-BODY FINITE-SIZE ERRORS IN METALS

Here, we provide an analysis of asymptotic finite-size errors in metals, based on the uniform electron gas (UEG). The potential energy (per electron) of the UEG can be expressed via the Coulomb interaction  $v(q) = 4\pi e^2/q^2$  and the structure factor  $S(q)$  [7],

$$U = \frac{1}{2} \int \frac{d^3q}{(2\pi)^3} v(q) [S(q) - 1] = \frac{e^2}{\pi} \int_0^\infty dq [S(q) - 1]. \quad (\text{S5})$$

The exact long wavelength behavior of the structure factor is  $S(q) = \hbar q^2/2m\omega_p$ , where  $\omega_p = \sqrt{4\pi n e^2/m}$  is the plasmon frequency; we expect all correlated methods that include the physics of the RPA capture this long wavelength behavior. In numerical calculations of finite systems with periodic boundary conditions, momentum transfers near  $q = 0$  are neglected, and so we can estimate the finite-size error as

$$\Delta U = \frac{e^2}{\pi} \int_0^{q_c} dq S(q) \approx \frac{\hbar e^2}{6m\pi\omega_p} q_c^3 \quad (\text{S6})$$

where

$$q_c = \left(\frac{3}{4\pi}\right)^{1/3} \frac{2\pi}{L} = (6\pi^2 n)^{1/3} N^{-1/3} = 2^{1/3} k_F N^{-1/3} \quad (\text{S7})$$

is the radius of a sphere with volume  $(2\pi)^3/V$ . Therefore, the finite-size error of the potential energy is  $O(N^{-1})$ . This analysis assumes that the structure factor itself has no finite-size error.

However, the *correlation* energy is the difference between the interacting and noninteracting (Hartree-Fock) energies,

$$E_c = \frac{e^2}{\pi} \int_0^\infty dq [S(q) - S^{(0)}(q)]. \quad (\text{S8})$$

In contrast to the behavior of interacting theories, the long wavelength behavior of the noninteracting structure factor is  $S^{(0)}(q) = 3q/4k_F$ , such that the finite-size error of the mean-field potential energy is  $O(q_c^2) \sim O(N^{-2/3})$ . Therefore, in principle, the correlation energy inherits this finite-size error and it vanishes as  $N^{-2/3}$  in the large  $N$  limit. Specifically, using these leading-order terms in both the exact interacting and noninteracting structure factors, we can estimate the finite-size error as

$$\Delta E_c = \frac{\hbar e^2}{6m\pi\omega_p} q_c^3 - \frac{3e^2}{8\pi k_F} q_c^2, \quad (\text{S9})$$

which is functionally equivalent to Eq. (S4).

As a tractable demonstration of this behavior, we consider the textbook RPA correlation energy,

$$E_c^{(\text{RPA})} = \lim_{q_c \rightarrow 0} E_c^{(\text{RPA})}(q_c), \quad E_c^{(\text{RPA})}(q_c) = \frac{\hbar}{2\pi n} \int_{q_c}^{\infty} \frac{4\pi q^2 dq}{(2\pi)^3} \int_0^{\infty} d\omega \left\{ \ln \left[ 1 - v(q)\chi^{(0)}(q, i\omega) \right] + v(q)\chi^{(0)}(q, i\omega) \right\}, \quad (\text{S10})$$

which can be evaluated by simple two-dimensional quadrature and  $\chi^{(0)}(q, i\omega)$  is the Lindhard function. Again, we emphasize that the first term (containing the logarithm) is the RPA potential energy, and second first term only serves to remove the Hartree-Fock exchange energy, as needed for the definition of the correlation energy. At small  $q_c$ , the second (exchange) term dominates and upon integration yields  $E_c^{(\text{RPA})}(q_c) \sim q_c^2 \sim N^{-2/3}$ .

This behavior is confirmed numerically, and the result is shown in Fig. S3 (left) for the UEG at  $r_s = 4$ . We see that the analytic expression (evaluated by numerical integration) converges to the TDL with the expected form. However, the asymptotic behavior (linear in  $N^{-2/3}$ ) is only observed for large system sizes with  $N \gtrsim 100$ . We show that the same behavior persists for plane-wave based calculations performed in the manner of Sec. S1. Fitting the correlation energy to Eq. (S4) using four data points (with  $b = 0$ ) or with six data points (with  $b \neq 0$ ) gives predictions that are in excellent agreement with exact RPA result. We also show the CCSD TDL convergence in Fig. S3 (right) and similarly see that the fits with  $b = 0$  and  $b \neq 0$  agree well with each other. In principle, Eqs. (S9) or (S10) could also be used effectively as finite-size *corrections*, although we do not do so here.

### S3. ATOMISTIC SOLID LITHIUM CALCULATIONS

#### A. Calculation details

Except where otherwise stated, all calculation details, including basis sets and pseudopotentials, are the same as in Ref. [8]. The CCSD data is taken from Ref. [8], but using  $N^{-2/3}$  extrapolation to the TDL, as discussed in Sec. S2. As seen in Tab. S3, this difference causes only small changes to our predicted properties. Calculation details for bulk DCSD are similar to those from CCSD [8], except again for the TDL extrapolation. The single atom DCSD correlation energies were found using two shells of ghost atoms in a molecular calculation.

As in our UEG study, the CC energies with triple excitations are estimated via their differences to DCSD energies calculated with the same system size. Specifically, calculations with triple excitations were performed on an 8-atom supercell with  $\Gamma$ -point sampling (equivalent to sampling with four  $k$  points on a two atom cubic unit cell) and 1s core electrons frozen. An additional calculation was performed on a 16-atom cubic supercell at lattice parameter 3.5 Å using frozen virtual natural orbitals. The difference with respect to a calculation on the 8-atom supercell with the same frozen virtual treatment was used as an additional finite-size correction. At each basis set, the difference between the triple calculation and DCSD at this system size was added to the DCSD energy at that basis set in the TDL. Correlation energies were extrapolated to the CBS limit using a  $X^{-3}$  form ( $X = 3, 4$  for TZ, QZ) [9]. After the TDL CBS results for each coupled cluster variant were estimated, as in Ref. [8], the Birch-Murnaghan [10, 11] equation-of-state was fit to extract the lattice parameter, bulk modulus, and cohesive energy.

#### B. Final results

Table S3 shows our calculated structural and energetic properties of lithium, i.e., lattice parameter  $a$ , bulk modulus  $B$ , and cohesive energy  $E_{\text{coh}}$ .

	$a$ (Å)	$B$ (GPa)	$E_{\text{coh}}$ (m $E_h$ )
CCSD ( $N^{-1}$ ) [8]	3.49	12.8	-51
CCSD	3.48	13.0	-52
DCSD	3.47	13.2	-55
ring-CCSDT	3.46	13.1	-57
CCSDT	3.47	13.3	-57
DCSDT	3.47	13.2	-57
Experiment [11–14]	3.45	13.3	-61

TABLE S3. Equilibrium lattice parameter  $a$ , bulk modulus  $B$  and cohesive energy  $E_{\text{coh}}$  for bulk BCC Li. Shown are CCSD with a  $N^{-1}$  TDL extrapolation from a previous study [8], CCSD (with a  $N^{-2/3}$  extrapolation), DCSD, ring-CCSDT, CCSDT, and DCSDT as well as zero-point motion corrected experimental results [11–14].

- 
- [1] A. Baldereschi, Mean-Value Point in the Brillouin Zone, *Phys. Rev. B* **7**, 5212 (1973).
- [2] J. J. Shepherd and A. Grüneis, Many-Body Quantum Chemistry for the Electron Gas: Convergent Perturbative Theories, *Phys. Rev. Lett.* **110**, 226401 (2013).
- [3] J. J. Shepherd, T. M. Henderson, and G. E. Scuseria, Range-Separated Brueckner Coupled Cluster Doubles Theory, *Phys. Rev. Lett.* **112**, 133002 (2014).
- [4] J. J. Shepherd, T. M. Henderson, and G. E. Scuseria, Coupled cluster channels in the homogeneous electron gas, *J. Chem. Phys.* **140**, 124102 (2014).
- [5] J. P. Perdew and A. Zunger, Self-interaction correction to density-functional approximations for many-electron systems, *Phys. Rev. B* **23**, 5048 (1981).
- [6] D. M. Ceperley and B. J. Alder, Ground State of the Electron Gas by a Stochastic Method, *Phys. Rev. Lett.* **45**, 566 (1980).
- [7] G. F. Giuliani and G. Vignale, *Quantum Theory of the Electron Liquid*, 1st ed. (Cambridge University Press, Cambridge/New York, 2005).
- [8] V. A. Neufeld, H.-Z. Ye, and T. C. Berkelbach, Ground-State Properties of Metallic Solids from Ab Initio Coupled-Cluster Theory, *J. Phys. Chem. Lett.* **13**, 7497 (2022).
- [9] T. Helgaker, W. Klopper, H. Koch, and J. Noga, Basis-set convergence of correlated calculations on water, *J. Chem. Phys.* **106**, 9639 (1997).
- [10] F. Birch, Finite elastic strain of cubic crystals, *Phys. Rev.* **71**, 809 (1947).
- [11] G.-X. Zhang, A. M. Reilly, A. Tkatchenko, and M. Scheffler, Performance of various density-functional approximations for cohesive properties of 64 bulk solids, *New J. Phys.* **20**, 063020 (2018).
- [12] R. Berliner and S. A. Werner, Effect of stacking faults on diffraction: The structure of lithium metal, *Phys. Rev. B* **34**, 3586 (1986).
- [13] R. A. Felice, J. Trivisonno, and D. E. Schuele, Temperature and pressure dependence of the single-crystal elastic constants of Li 6 and natural lithium, *Phys. Rev. B* **16**, 5173 (1977).
- [14] C. Kittel, *Introduction to solid state physics*, 8th ed. (John Wiley & Sons, Inc., 2005).

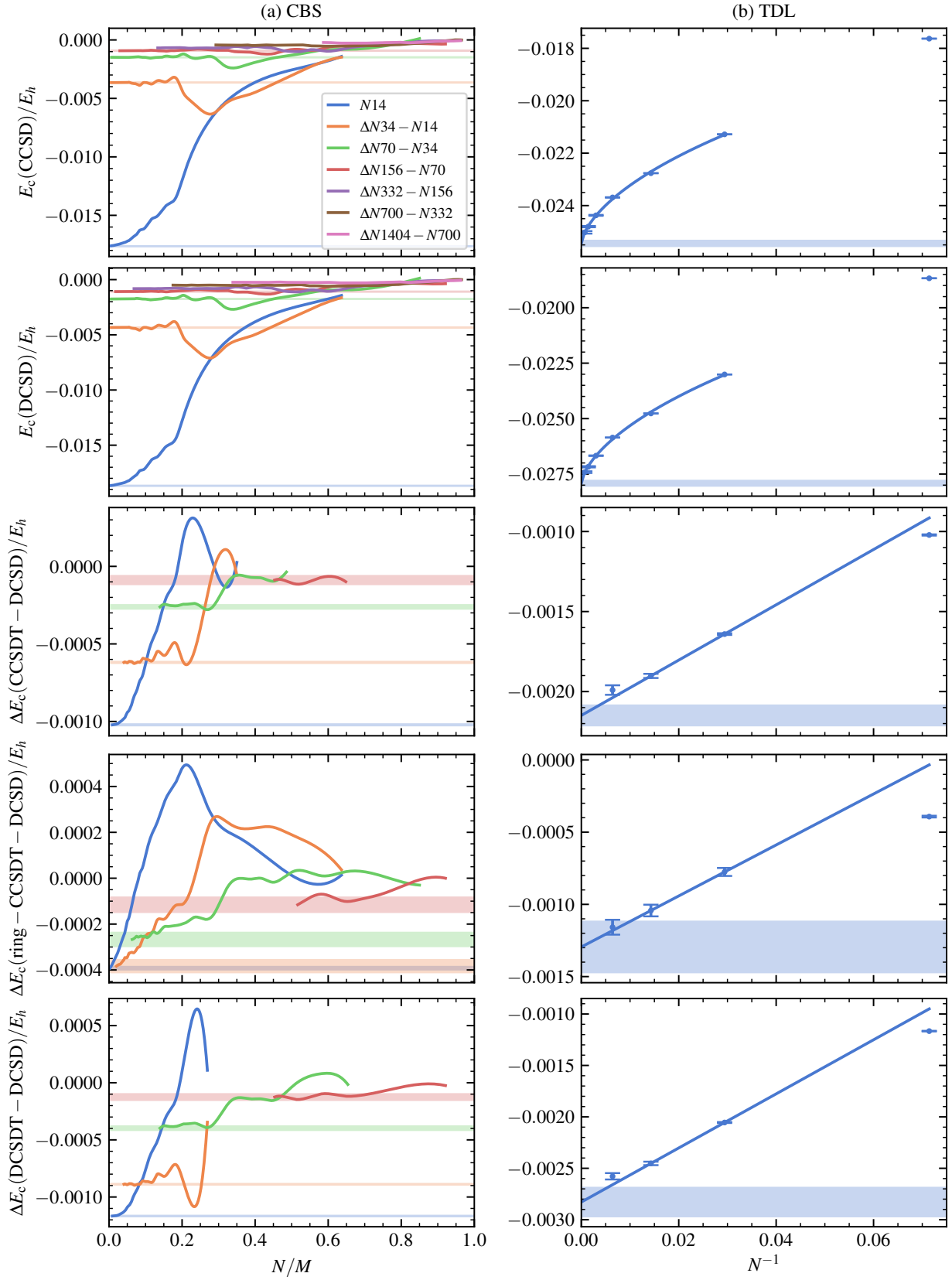


FIG. S2. Convergence to (a) complete basis set (CBS) limit and (b) thermodynamic limit (TDL) for the uniform electron gas at  $r_s = 4$ . CCSD and DCSD correlation energies are shown, as well as CCSDT, ring-CCSDT, and DCSDT energy differences to that of DCSD. Estimated values with error bars are shown with shaded regions.

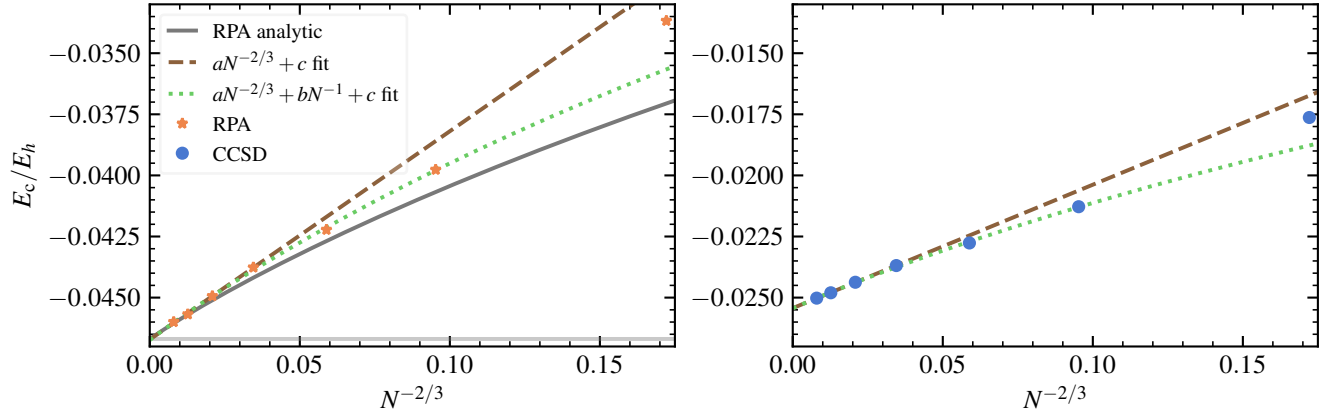


FIG. S3. Thermodynamic limit convergence of the RPA (left) and CCSD (right) correlation energy at  $r_s = 4$ . We show the numerical correlation energy from plane-wave based calculations (orange stars and blue circles). Two fits are tested on the results. For RPA, we also show the analytic correlation energy from Eq. (S10) (dark grey solid curve) and a horizontal line at the exact RPA correlation energy in the TDL.